



Detection of change in cancer breast tissues from fractal indicators:
A brief introduction

Journées RT² ANAIS & MAIAGES

Aléatoire et Fractales à Vannes

April 2, 2025

Barbara Pascal

CompuMAINE:* K. Batchelder, A. Khalil, B. G. White

Laboratoire des Sciences du Numérique de Nantes: B. Pascal

Laboratoire de Physique ENSL: P. Abry, B. Audit, L. Davy, N. Pustelnik

* Computational Modeling, Analysis of Imagery and Numerical Experiments

Breast cancer:

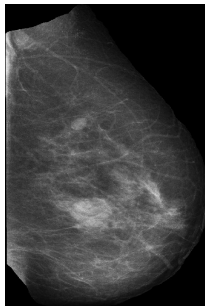
- most common cancer amongst women with ~ 1 over 8 diagnosed
- early detection is critical for the patient's survival

Context and motivations

Breast cancer:

- most common cancer amongst women with ~ 1 over 8 diagnosed
- early detection is critical for the patient's survival

X-ray imaging: most used imaging technique yielding a so-called *mammogram*

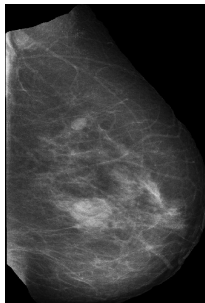


Context and motivations

Breast cancer:

- most common cancer amongst women with ~ 1 over 8 diagnosed
- early detection is critical for the patient's survival

X-ray imaging: most used imaging technique yielding a so-called *mammogram*



Assessment by a radiologist:

- fatty tissues: translucent to X-rays (black)
- epithelial and stromal tissues: absorb X-rays (white)
- tumorous tissues: **also absorb X-rays** (white)

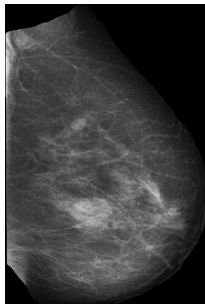
⇒ errors of both I and II types

Context and motivations

Breast cancer:

- most common cancer amongst women with ~ 1 over 8 diagnosed
- early detection is critical for the patient's survival

X-ray imaging: most used imaging technique yielding a so-called *mammogram*



Assessment by a radiologist:

- fatty tissues: translucent to X-rays (black)
- epithelial and stromal tissues: absorb X-rays (white)
- tumorous tissues: **also absorb X-rays** (white)

⇒ errors of both I and II types

Computer-Aided Detection: used in 92% of screening mammograms in the U.S.

Tissue density fluctuations in normal vs. cancerous breasts

Breast Imaging Reporting And Data System (BI-RADS): four categories

- I: Almost entirely fatty tissue (10% of women in U.S.)
- II: Scattered areas of density (40% of women in U.S.)
- III: Heterogeneous density (40% of women in U.S.)
- IV: Extremely dense (10% of women in U.S.)

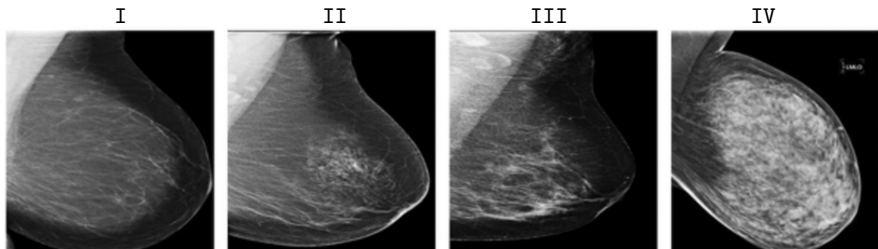
(C. Balleyguier et al., 2007, Eur. J. Radiol.)

Tissue density fluctuations in normal vs. cancerous breasts

Breast Imaging Reporting And Data System (BI-RADS): four categories

- I: Almost entirely fatty tissue (10% of women in U.S.)
- II: Scattered areas of density (40% of women in U.S.)
- III: Heterogeneous density (40% of women in U.S.)
- IV: Extremely dense (10% of women in U.S.)

(C. Balleyguier et al., 2007, Eur. J. Radiol.)



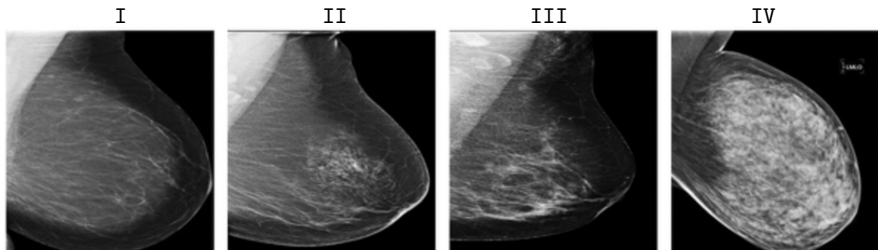
Source: B. White, 2023, *Electronic Theses and Dissertations, University of Maine.*

Tissue density fluctuations in normal vs. cancerous breasts

Breast Imaging Reporting And Data System (BI-RADS): four categories

- I: Almost entirely fatty tissue (10% of women in U.S.)
- II: Scattered areas of density (40% of women in U.S.)
- III: Heterogeneous density (40% of women in U.S.)
- IV: Extremely dense (10% of women in U.S.)

(C. Balleyguier et al., 2007, Eur. J. Radiol.)



Source: B. White, 2023, *Electronic Theses and Dissertations, University of Maine.*

Overall mammographic density: (S. S. Nazari et al., 2018, *Breast cancer*)

⇒ important **risk factor** for breast cancer radiological assessment

BI-RADS limitations:

- subjective, with both inter- and intra-observer variability
- classification in four classes not reflecting continuous changes in tissues

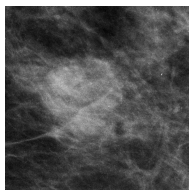
Quantitative assessment of breast density based on fractal properties

BI-RADS limitations:

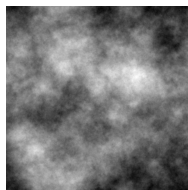
- subjective, with both inter- and intra-observer variability
- classification in four classes not reflecting continuous changes in tissues

Self-similar isotropic random fields: $f(\mathbf{x}_0 + \lambda \mathbf{u}) - f(\mathbf{x}_0) \stackrel{(\text{law})}{\simeq} \lambda^H (f(\mathbf{x}_0 + \mathbf{u}) - f(\mathbf{x}_0))$

Mammogram



fractal random field



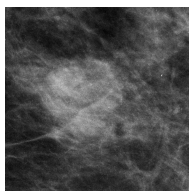
Quantitative assessment of breast density based on fractal properties

BI-RADS limitations:

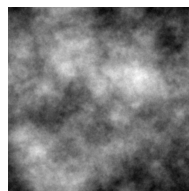
- subjective, with both inter- and intra-observer variability
- classification in four classes not reflecting continuous changes in tissues

Self-similar isotropic random fields: $f(\mathbf{x}_0 + \lambda\mathbf{u}) - f(\mathbf{x}_0) \stackrel{(\text{law})}{\simeq} \lambda^H (f(\mathbf{x}_0 + \mathbf{u}) - f(\mathbf{x}_0))$

Mammogram



fractal random field



Self-similar textures: fractal analysis, e.g., fractal dimension of a rough surface, for

- classification of mammogram density (Caldwell et al., 1990, *Phys. Med. Biol.*)
- lesion detection in mammograms (Burgess et al., 2001, *Med. Biol.*)
- assessment of breast cancer risk (Heine et al., 2002, *Acad. Radiol.*)

Physiological motivations and goals

Breast **microenvironment** plays a crucial role in tumorigenesis:

- structure integrity preserved \implies lesions are suppressed
- structure lost by tissue disruption \implies tumor is promoted

Tumor vs. healthy not only in tumor but more fundamentally in surrounding tissue

Physiological motivations and goals

Breast **microenvironment** plays a crucial role in tumorigenesis:

- structure integrity preserved \implies lesions are suppressed
- structure lost by tissue disruption \implies tumor is promoted

Tumor vs. healthy not only in tumor but more fundamentally in surrounding tissue

Pioneer work: Marin et al., 2017, *Med. Phys.* quantitatively and objectively assessed

- tissue disruption
- loss of homeostasis in breast tissue microenvironment
- bilateral asymmetry

via wavelet-based mammogram local analysis.

Physiological motivations and goals

Breast **microenvironment** plays a crucial role in tumorigenesis:

- structure integrity preserved \implies lesions are suppressed
- structure lost by tissue disruption \implies tumor is promoted

Tumor vs. healthy not only in tumor but more fundamentally in surrounding tissue

Pioneer work: Marin et al., 2017, *Med. Phys.* quantitatively and objectively assessed

- tissue disruption
- loss of homeostasis in breast tissue microenvironment
- bilateral asymmetry

via wavelet-based mammogram local analysis.

Main idea: quantify density fluctuations through the Hölder exponent $h(x_0)$ probed via
multifractal formalism based on 2D Wavelet Transform Modulus Maxima
 \implies risk assessment and tumorous breasts detection without seeing a tumor

A very short reminder about fractional Brownian fields

fBf of Hurst exponent $H \in [0, 1]$ denoted $\{B_H(\mathbf{x}), \mathbf{x} \in \mathbb{R}^2\}$

- Gaussian field with zero-mean
- and for some $\sigma^2 > 0$, correlation function writing

$$\mathbb{E}[B_H(\mathbf{x})B_H(\mathbf{y})] = \frac{\sigma^2}{2} (\|\mathbf{x}\|^{2H} + \|\mathbf{y}\|^{2H} - \|\mathbf{x} - \mathbf{y}\|^{2H})$$

A very short reminder about fractional Brownian fields

fBf of Hurst exponent $H \in [0, 1]$ denoted $\{B_H(\mathbf{x}), \mathbf{x} \in \mathbb{R}^2\}$

- Gaussian field with zero-mean
- and for some $\sigma^2 > 0$, correlation function writing

$$\mathbb{E}[B_H(\mathbf{x})B_H(\mathbf{y})] = \frac{\sigma^2}{2} (\|\mathbf{x}\|^{2H} + \|\mathbf{y}\|^{2H} - \|\mathbf{x} - \mathbf{y}\|^{2H})$$

Stationary increments

$$\begin{aligned} \forall \mathbf{u} \in \mathbb{R}^2, \quad & \mathbb{E}[(B_H(\mathbf{x} + \mathbf{u}) - B_H(\mathbf{x}))(B_H(\mathbf{y} + \mathbf{u}) - B_H(\mathbf{y}))] \\ &= \|\mathbf{x} + \mathbf{u} - \mathbf{y}\|^{2H} + \|\mathbf{x} - \mathbf{u} - \mathbf{y}\|^{2H} - 2\|\mathbf{x} - \mathbf{y}\|^{2H} \end{aligned}$$

A very short reminder about fractional Brownian fields

fBf of Hurst exponent $H \in [0, 1]$ denoted $\{B_H(\mathbf{x}), \mathbf{x} \in \mathbb{R}^2\}$

- Gaussian field with zero-mean
- and for some $\sigma^2 > 0$, correlation function writing

$$\mathbb{E}[B_H(\mathbf{x})B_H(\mathbf{y})] = \frac{\sigma^2}{2} (\|\mathbf{x}\|^{2H} + \|\mathbf{y}\|^{2H} - \|\mathbf{x} - \mathbf{y}\|^{2H})$$

Stationary increments

$$\begin{aligned} \forall \mathbf{u} \in \mathbb{R}^2, \quad & \mathbb{E}[(B_H(\mathbf{x} + \mathbf{u}) - B_H(\mathbf{x}))(B_H(\mathbf{y} + \mathbf{u}) - B_H(\mathbf{y}))] \\ &= \|\mathbf{x} + \mathbf{u} - \mathbf{y}\|^{2H} + \|\mathbf{x} - \mathbf{u} - \mathbf{y}\|^{2H} - 2\|\mathbf{x} - \mathbf{y}\|^{2H} \end{aligned}$$

$$\begin{aligned} \text{For } \|\mathbf{u}\| \ll \|\mathbf{x} - \mathbf{y}\|, \quad & \mathbb{E}[(B_H(\mathbf{x} + \mathbf{u}) - B_H(\mathbf{x}))(B_H(\mathbf{y} + \mathbf{u}) - B_H(\mathbf{y}))] \\ &= \|\mathbf{x} - \mathbf{y}\|^{2(H-1)} 2H(2H-1) \|\mathbf{u}\|^2 + o(\|\mathbf{u}\|^2) \end{aligned}$$

A very short reminder about fractional Brownian fields

fBf of Hurst exponent $H \in [0, 1]$ denoted $\{B_H(\mathbf{x}), \mathbf{x} \in \mathbb{R}^2\}$

- Gaussian field with zero-mean
- and for some $\sigma^2 > 0$, correlation function writing

$$\mathbb{E}[B_H(\mathbf{x})B_H(\mathbf{y})] = \frac{\sigma^2}{2} (\|\mathbf{x}\|^{2H} + \|\mathbf{y}\|^{2H} - \|\mathbf{x} - \mathbf{y}\|^{2H})$$

Stationary increments

$$\begin{aligned} \forall \mathbf{u} \in \mathbb{R}^2, \quad & \mathbb{E}[(B_H(\mathbf{x} + \mathbf{u}) - B_H(\mathbf{x}))(B_H(\mathbf{y} + \mathbf{u}) - B_H(\mathbf{y}))] \\ &= \|\mathbf{x} + \mathbf{u} - \mathbf{y}\|^{2H} + \|\mathbf{x} - \mathbf{u} - \mathbf{y}\|^{2H} - 2\|\mathbf{x} - \mathbf{y}\|^{2H} \end{aligned}$$

$$\begin{aligned} \text{For } \|\mathbf{u}\| \ll \|\mathbf{x} - \mathbf{y}\|, \quad & \mathbb{E}[(B_H(\mathbf{x} + \mathbf{u}) - B_H(\mathbf{x}))(B_H(\mathbf{y} + \mathbf{u}) - B_H(\mathbf{y}))] \\ &= \|\mathbf{x} - \mathbf{y}\|^{2(H-1)} 2H(2H-1) \|\mathbf{u}\|^2 + o(\|\mathbf{u}\|^2) \end{aligned}$$

- $H < 1/2$: anti-correlated
- $H = 1/2$: uncorrelated \implies disruption
- $H > 1/2$: long-range correlated

A very short reminder about fractional Brownian fields

Self-similarity

$$\forall \mathbf{x}_0 \in \mathbb{R}^2, \lambda > 0, \quad B_H(\mathbf{x}_0 + \lambda \mathbf{x}) - B_H(\mathbf{x}_0) \stackrel{\text{(law)}}{\simeq} \lambda^H (B_H(\mathbf{x}_0 + \mathbf{x}) - B_H(\mathbf{x}_0)) \text{ in } \mathcal{V}(\mathbf{x}_0)$$

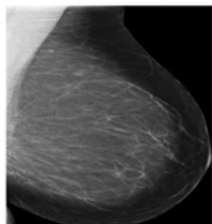
A very short reminder about fractional Brownian fields

Self-similarity

$$\forall \mathbf{x}_0 \in \mathbb{R}^2, \lambda > 0, \quad B_H(\mathbf{x}_0 + \lambda \mathbf{x}) - B_H(\mathbf{x}_0) \stackrel{\text{(law)}}{\simeq} \lambda^H (B_H(\mathbf{x}_0 + \mathbf{x}) - B_H(\mathbf{x}_0)) \text{ in } \mathcal{V}(\mathbf{x}_0)$$

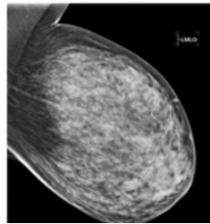
The larger the Hurst exponent H , the smoother the texture.

I: fatty tissues



$$H \simeq 0.30$$

IV: dense tissues

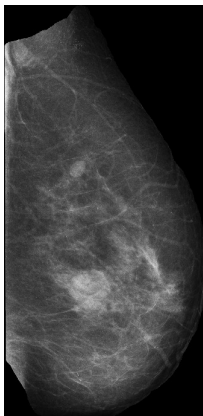


$$H \simeq 0.65$$

(Kestener et al., 2001, *Image Anal. Stereol.*)

Local fractal analysis of mammographic breast tissue

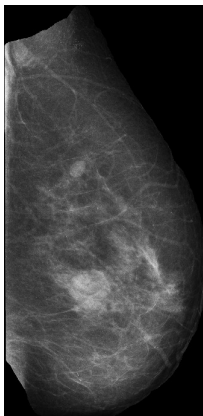
CompuMAINE local mammogram analysis ([Marin et al., 2017, *Phys. Med. Biol.*](#))



Local fractal analysis of mammographic breast tissue

CompuMAINE local mammogram analysis (Marin et al., 2017, *Phys. Med. Biol.*)

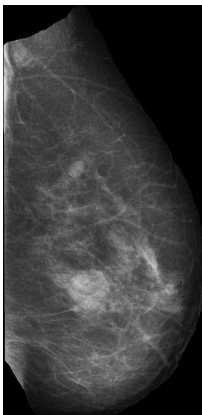
- $H < 1/2$ monofractal anti-correlated: fatty tissues (healthy)



Local fractal analysis of mammographic breast tissue

CompuMAINE local mammogram analysis (Marin et al., 2017, *Phys. Med. Biol.*)

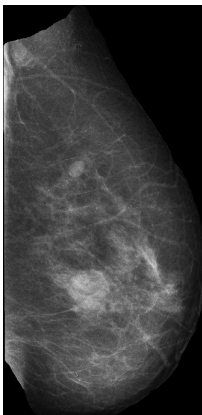
- $H < 1/2$ monofractal anti-correlated: fatty tissues (healthy)
- $H > 1/2$ monofractal long-range correlated: dense tissues (healthy)



Local fractal analysis of mammographic breast tissue

CompuMAINE local mammogram analysis (Marin et al., 2017, *Phys. Med. Biol.*)

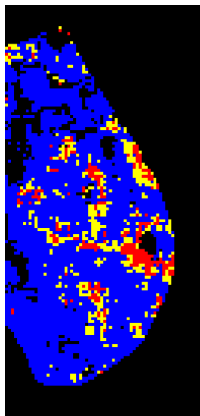
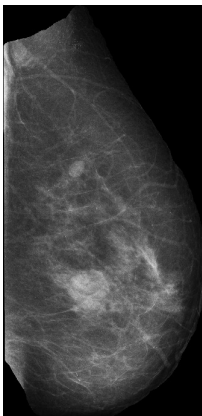
- $H < 1/2$ monofractal anti-correlated: fatty tissues (healthy)
- $H > 1/2$ monofractal long-range correlated: dense tissues (healthy)
- $H \simeq 1/2$ monofractal uncorrelated: disrupted tissues (tumorous)



Local fractal analysis of mammographic breast tissue

CompuMAINE local mammogram analysis (Marin et al., 2017, *Phys. Med. Biol.*)

- $H < 1/2$ monofractal anti-correlated: fatty tissues (healthy)
- $H > 1/2$ monofractal long-range correlated: dense tissues (healthy)
- $H \simeq 1/2$ monofractal uncorrelated: disrupted tissues (tumorous)



Assessment of the role of disruption in tumor promotion

Dataset: University of South Florida, Digital Database for Screening Mammography

- Mediolateral oblique views only;
- 43 normal, 49 cancer, 35 benign;
- for benign and cancer microcalcification only, masses excluded;

Image sliding-window analysis:

- squared 360×360 -pixel window
- with 32-pixel horizontal and vertical shifts
 \Rightarrow analysis of all 360×360 -pixel overlapping patches

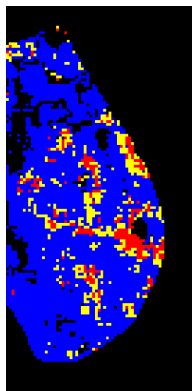
Example: mammogram of size 4459×2155 pixels

4457 patches \iff 4457 measures of the roughness H

Cancer risk metric: number of yellow patches

$H \sim 1/2$: disrupted tissues

\Rightarrow more **specific** than BI-RADS and **quantitative**



Assessment of the role of disruption in tumor promotion

Q.: Is the quantity of disrupted tissues, $H \simeq 1/2$, indicative of a tumorous breast?

Assessment of the role of disruption in tumor promotion

Q.: Is the quantity of disrupted tissues, $H \simeq 1/2$, indicative of a tumorous breast?

Wilcoxon rank test a.k.a. Wilcoxon-Mann-Whitney

Independent sets of real numbers X and Y , of cardinalities n_x and n_y respectively

$$H_0: \mathbb{P}(X > Y) = \mathbb{P}(Y > X)$$

Assessment of the role of disruption in tumor promotion

Q.: Is the quantity of disrupted tissues, $H \simeq 1/2$, indicative of a tumorous breast?

Wilcoxon rank test a.k.a. Wilcoxon-Mann-Whitney

Independent sets of real numbers X and Y , of cardinalities n_x and n_y respectively

$$\mathsf{H0}: \mathbb{P}(X > Y) = \mathbb{P}(Y > X)$$

- (i) order elements of $X \cup Y$ to form an increasing sequence;
- (ii) assign to each element in $X \cup Y$ its *rank* in the sequence;
- (iii) sum the ranks of elements in X : variable S_x .

Assessment of the role of disruption in tumor promotion

Q.: Is the quantity of disrupted tissues, $H \simeq 1/2$, indicative of a tumorous breast?

Wilcoxon rank test a.k.a. Wilcoxon-Mann-Whitney

Independent sets of real numbers X and Y , of cardinalities n_x and n_y respectively

$$\mathbf{H0}: \mathbb{P}(X > Y) = \mathbb{P}(Y > X)$$

- (i) order elements of $X \cup Y$ to form an increasing sequence;
- (ii) assign to each element in $X \cup Y$ its *rank* in the sequence;
- (iii) sum the ranks of elements in X : variable S_x .

If at least 20 samples, law of S_x well approximated by a Gaussian with

$$\mu = n_x n_y / 2; \quad \sigma^2 = n_x n_y (n_x + n_y + 1) / 2.$$

If $|S_x - \mu|/\sigma > 1.96$, **H0** is rejected with confidence level $\alpha = 0.05$.

Assessment of the role of disruption in tumor promotion

Q.: Is the quantity of disrupted tissues, $H \simeq 1/2$, indicative of a tumorous breast?

Wilcoxon rank test a.k.a. Wilcoxon-Mann-Whitney

Independent sets of real numbers X and Y , of cardinalities n_x and n_y respectively

$$\mathbf{H0}: \mathbb{P}(X > Y) = \mathbb{P}(Y > X)$$

- (i) order elements of $X \cup Y$ to form an increasing sequence;
- (ii) assign to each element in $X \cup Y$ its *rank* in the sequence;
- (iii) sum the ranks of elements in X : variable S_x .

If at least 20 samples, law of S_x well approximated by a Gaussian with

$$\mu = n_x n_y / 2; \quad \sigma^2 = n_x n_y (n_x + n_y + 1) / 2.$$

If $|S_x - \mu|/\sigma > 1.96$, **H0** is rejected with confidence level $\alpha = 0.05$.

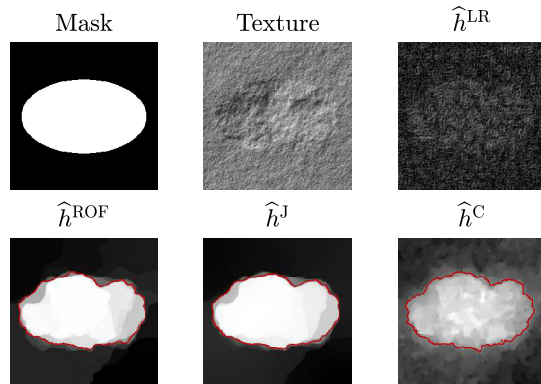
Tumorous breasts have **more disrupted tissues**: normal vs. tumor: $P \sim 0.0006$

In details, normal vs. cancer: $P \sim 0.0023$, normal vs. benign: $P \sim 0.0049$.

Fractal features piecewise constant estimation from leaders

Séminaire Cristolien d'Analyse Multifractale: February 4, 2021 (*online*)

bpascal-fr.github.io/assets/pdfs/SCAM21.pdf



⇒ estimation of local Hölder exponent $h(x)$ at the **pixel** level from **wavelet leaders**

(Pascal et al., 2020, *Ann. Telecommun.*; Pascal et al., 2021, *Appl. Comput. Harmon. Anal.*;
Pascal et al., 2021, *J. Math. Imaging Vis.*)

Patch-wise fractal analysis of mammographic breast tissue

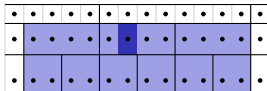
But first: assess that **wavelet leaders formalism** agrees with UMaine analyzes

Patch-wise fractal analysis of mammographic breast tissue

But first: assess that **wavelet leaders formalism** agrees with UMaine analyzes

Wavelet leaders: $\mathcal{L}_{a,n}$ at scale a and pixel n supremum of wavelet coefficients

- at all finer scales $a' \leq a$
- in a spatial neighborhood

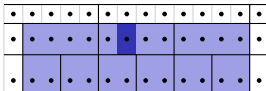


Patch-wise fractal analysis of mammographic breast tissue

But first: assess that **wavelet leaders formalism** agrees with UMaine analyzes

Wavelet leaders: $\mathcal{L}_{a,\underline{n}}$ at scale a and pixel \underline{n} supremum of wavelet coefficients

- at all finer scales $a' \leq a$
- in a spatial neighborhood



For a grid of pixels $\Omega \subset \mathbb{R}^2$, scaling exponent $\zeta(q)$ accessible through

$$\frac{1}{|\Omega|} \sum_{\underline{n} \in \Omega} \mathcal{L}_{a,\underline{n}}^q = F_q a^{\zeta(q)}, \quad a \rightarrow 0^+$$

homogeneous monofractal texture of Hurst exponent $H \implies \zeta(q) = qH$

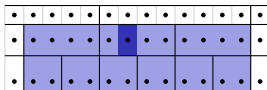
(Wendt et al., 2007, *IEEE Signal Process. Mag.*)

Patch-wise fractal analysis of mammographic breast tissue

But first: assess that **wavelet leaders formalism** agrees with UMaine analyzes

Wavelet leaders: $\mathcal{L}_{a,n}$ at scale a and pixel n supremum of wavelet coefficients

- at all finer scales $a' \leq a$
- in a spatial neighborhood



For a grid of pixels $\Omega \subset \mathbb{R}^2$, scaling exponent $\zeta(q)$ accessible through

$$\frac{1}{|\Omega|} \sum_{n \in \Omega} \mathcal{L}_{a,n}^q = F_q a^{\zeta(q)}, \quad a \rightarrow 0^+$$

homogeneous monofractal texture of Hurst exponent $H \implies \zeta(q) = qH$

(Wendt et al., 2007, *IEEE Signal Process. Mag.*)

\implies linear regression to estimate H for all 360×360 -pixel overlapping patches

Patch-wise fractal analysis of mammographic breast tissue

Wavelet leader coefficients (Wendt et al., 2009, Sig. Process.)

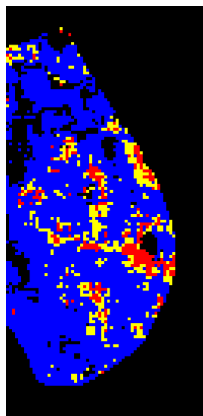
- $H < 1/2$ monofractal anti-correlated: fatty tissues (healthy)
- $H > 1/2$ monofractal long-range correlated: dense tissues (healthy)
- $H \simeq 1/2$ monofractal uncorrelated: disrupted tissues (tumorous)

Patch-wise fractal analysis of mammographic breast tissue

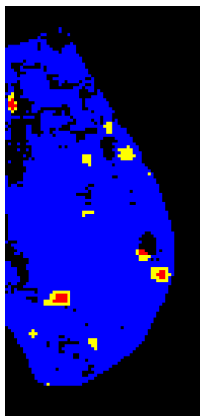
Wavelet leader coefficients (Wendt et al., 2009, Sig. Process.)

- $H < 1/2$ monofractal anti-correlated: fatty tissues (healthy)
- $H > 1/2$ monofractal long-range correlated: dense tissues (healthy)
- $H \simeq 1/2$ monofractal uncorrelated: disrupted tissues (tumorous)

CompuMaine



Leaders

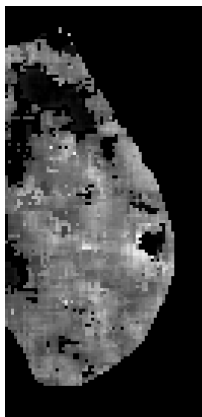


Patch-wise fractal analysis of mammographic breast tissue

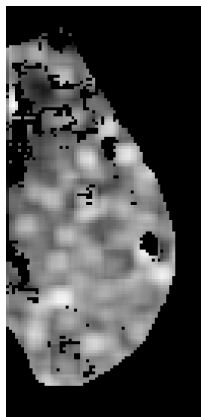
Wavelet leader coefficients (Wendt et al., 2009, Sig. Process.)

- $H < 1/2$ monofractal anti-correlated: fatty tissues (healthy)
- $H > 1/2$ monofractal long-range correlated: dense tissues (healthy)
- $H \simeq 1/2$ monofractal uncorrelated: disrupted tissues (tumorous)

CompuMaine



Leaders



Multifractal formalism: local Hölder regularity $h(x_0)$

$$|f(\mathbf{x}) - P_n(\mathbf{x} - \mathbf{x}_0)| \leq C|\mathbf{x} - \mathbf{x}_0|^{h(x_0)} \quad \text{for } \mathbf{x} \in \mathcal{V}(\mathbf{x}_0)$$

with P_n a polynomial of degree $n < h(x_0)$

Local isotropic scale invariance: $f(\mathbf{x}_0 + \lambda \mathbf{u}) - f(\mathbf{x}_0) \stackrel{\text{(law)}}{\simeq} \lambda^{h(x_0)} (f(\mathbf{x}_0 + \mathbf{u}) - f(\mathbf{x}_0))$

A general framework for texture analysis: multifractal formalism

Multifractal formalism: local Hölder regularity $h(x_0)$

$$|f(\mathbf{x}) - P_n(\mathbf{x} - \mathbf{x}_0)| \leq C|\mathbf{x} - \mathbf{x}_0|^{h(x_0)} \quad \text{for } \mathbf{x} \in \mathcal{V}(\mathbf{x}_0)$$

with P_n a polynomial of degree $n < h(x_0)$

Local isotropic scale invariance: $f(\mathbf{x}_0 + \lambda \mathbf{u}) - f(\mathbf{x}_0) \stackrel{\text{(law)}}{\simeq} \lambda^{h(x_0)} (f(\mathbf{x}_0 + \mathbf{u}) - f(\mathbf{x}_0))$

For $h(x_0) \in (0, 1)$ and cusp-like only singularities



$$h(x) \equiv h_1 = 0.9$$

$$h(x) \equiv h_2 = 0.3$$

A general framework for texture analysis: multifractal formalism

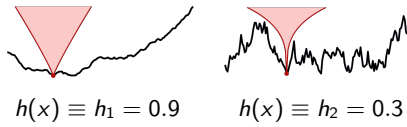
Multifractal formalism: **local** Hölder regularity $h(x_0)$

$$|f(\mathbf{x}) - P_n(\mathbf{x} - \mathbf{x}_0)| \leq C|\mathbf{x} - \mathbf{x}_0|^{h(x_0)} \quad \text{for } \mathbf{x} \in \mathcal{V}(\mathbf{x}_0)$$

with P_n a polynomial of degree $n < h(x_0)$

Local isotropic scale invariance: $f(\mathbf{x}_0 + \lambda \mathbf{u}) - f(\mathbf{x}_0) \stackrel{\text{(law)}}{\simeq} \lambda^{h(x_0)} (f(\mathbf{x}_0 + \mathbf{u}) - f(\mathbf{x}_0))$

For $h(x_0) \in (0, 1)$ and cusp-like only singularities



Singularity spectrum: $\mathcal{D}(h)$ Haussdorff dimension of $\{\mathbf{x} \in \mathbb{R}^2, h(\mathbf{x}) = h\}$

For a monofractal field, e.g., fractional Brownian field B_H : $h(\mathbf{x}_0) \equiv H$ and

$$\mathcal{D}(h) = \begin{cases} 2 & h = H \\ -\infty & h \neq H \end{cases}$$

Multifractal analysis of mammographic microenvironment

Kestener et al., 2001; Marin et al., 2017; Gerasimova-Chechkina et al., 2021

Multifractal analysis of mammographic microenvironment

Kestener et al., 2001; Marin et al., 2017; Gerasimova-Chechkina et al., 2021

2D Wavelet Transform: $\{f(\mathbf{x}), \mathbf{x} \in \mathbb{R}^2\}$ 2D-field

Smoothing function $\varphi(\mathbf{x}) \implies$ wavelets $\psi_1(\mathbf{x}) = \partial_{x_1} \varphi(x_1, x_2)$, $\psi_2(\mathbf{x}) = \partial_{x_2} \varphi(x_1, x_2)$

$$\mathbf{T}_\psi[f](\mathbf{b}, a) = \begin{pmatrix} a^{-2} \int \psi_1(a^{-1}(\mathbf{x} - \mathbf{b})) f(\mathbf{x}) d\mathbf{x} \\ a^{-2} \int \psi_2(a^{-1}(\mathbf{x} - \mathbf{b})) f(\mathbf{x}) d\mathbf{x} \end{pmatrix} \stackrel{\text{(complex)}}{=} \mathbf{M}_\psi[f](\mathbf{b}, a) \exp(i \mathbf{A}_\psi[f](\mathbf{b}, a))$$

Example: Gaussian and Mexican hat smoothing functions

$$\varphi_{\text{Gauss}}(\mathbf{x}) = \exp(-\|\mathbf{x}\|^2/2); \quad \varphi_{\text{Mex}}(\mathbf{x}) = (2 - \|\mathbf{x}\|^2) \exp(-\|\mathbf{x}\|^2/2)$$

leading respectively to $n_\psi = 1$ and $n_\psi = 3$ vanishing moments

Multifractal analysis using Wavelet Transform Modulus Maxima

Multifractal analysis of mammographic microenvironment

Kestener et al., 2001; Marin et al., 2017; Gerasimova-Chechkina et al., 2021

2D Wavelet Transform: $\{f(\mathbf{x}), \mathbf{x} \in \mathbb{R}^2\}$ 2D-field

Smoothing function $\varphi(\mathbf{x}) \implies$ wavelets $\psi_1(\mathbf{x}) = \partial_{x_1} \varphi(x_1, x_2)$, $\psi_2(\mathbf{x}) = \partial_{x_2} \varphi(x_1, x_2)$

$$\mathbf{T}_\psi[f](\mathbf{b}, a) = \begin{pmatrix} a^{-2} \int \psi_1(a^{-1}(\mathbf{x} - \mathbf{b})) f(\mathbf{x}) d\mathbf{x} \\ a^{-2} \int \psi_2(a^{-1}(\mathbf{x} - \mathbf{b})) f(\mathbf{x}) d\mathbf{x} \end{pmatrix} \stackrel{\text{(complex)}}{=} \mathbf{M}_\psi[f](\mathbf{b}, a) \exp(i \mathbf{A}_\psi[f](\mathbf{b}, a))$$

Example: Gaussian and Mexican hat smoothing functions

$$\varphi_{\text{Gauss}}(\mathbf{x}) = \exp(-\|\mathbf{x}\|^2/2); \quad \varphi_{\text{Mex}}(\mathbf{x}) = (2 - \|\mathbf{x}\|^2) \exp(-\|\mathbf{x}\|^2/2)$$

leading respectively to $n_\psi = 1$ and $n_\psi = 3$ vanishing moments

Wavelet Transform Modulus Maxima

$$\{(\mathbf{b}, a) \in \mathbb{R}^2, \times \mathbb{R}_+^* \mid \mathbf{M}_\psi[f](\mathbf{b}, a) \text{ locally maximal in direction } \mathbf{A}_\psi[f](\mathbf{b}, a)\}$$

Multifractal analysis using Wavelet Transform Modulus Maxima

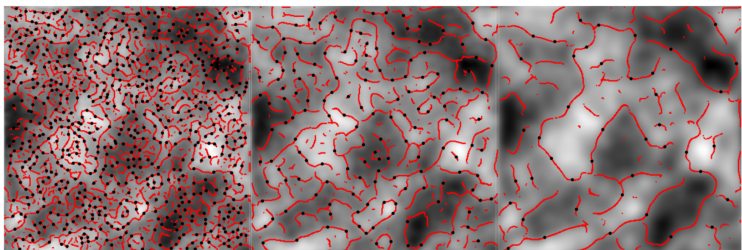


Figure 4.2: The maxima chains are shown for scales $a = 2^1\sigma_w$ (left), $a = 2^2\sigma_w$ (middle), and $a = 2^3\sigma_w$ (right) (where $\sigma_w = 7$ pixels) overlaid onto a 2D fBm image with $H = 0.5$. The local maxima along \mathcal{M}_ψ (WTMMM) are shown through small filled black dots.

Source: Basel G. White

Multifractal analysis using Wavelet Transform Modulus Maxima

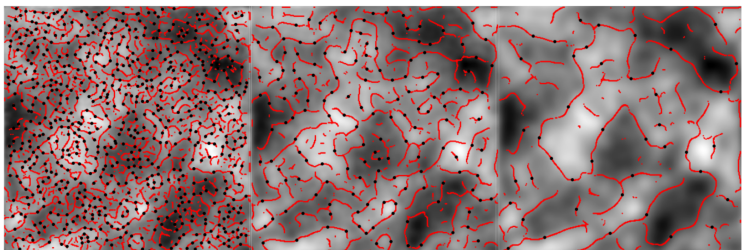


Figure 4.2: The maxima chains are shown for scales $a = 2^1\sigma_w$ (left), $a = 2^2\sigma_w$ (middle), and $a = 2^3\sigma_w$ (right) (where $\sigma_w = 7$ pixels) overlaid onto a 2D fBm image with $H = 0.5$. The local maxima along \mathcal{M}_ψ (WTMM) are shown through small filled black dots.

Source: Basel G. White

Wavelet Transform space-scale skeleton: $\mathcal{L}(a)$

lines formed by WTMM maxima across scales

Multifractal analysis using Wavelet Transform Modulus Maxima

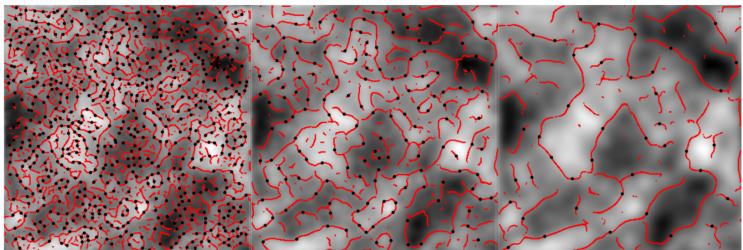


Figure 4.2: The maxima chains are shown for scales $a = 2^1\sigma_w$ (left), $a = 2^2\sigma_w$ (middle), and $a = 2^3\sigma_w$ (right) (where $\sigma_w = 7$ pixels) overlaid onto a 2D fBm image with $H = 0.5$. The local maxima along \mathcal{M}_ψ (WTMMM) are shown through small filled black dots.

Source: Basel G. White

Wavelet Transform space-scale skeleton: $\mathcal{L}(a)$

lines formed by WTMM maxima across scales

If a maxima line $\mathcal{L}_{x_0}(a)$ is pointing toward a singularity x_0 as $a \rightarrow 0^+$, then

$$\mathbf{M}_\psi[f](\mathcal{L}_{x_0}(a)) \sim a^{h(x_0)}, \quad a \rightarrow 0^+$$

provided that the wavelet has $n_\psi > h(x_0)$ vanishing moments.

Multifractal analysis using Wavelet Transform Modulus Maxima

Partition function: for a set $\mathcal{L}(a)$ of maxima lines

$$\mathcal{Z}(q, a) = \sum_{\ell \in \mathcal{L}(a)} \left(\sup_{(\mathbf{b}, a') \in \ell, a' \leq a} \mathbf{M}_\psi[f](\mathbf{b}, a') \right)^q$$

q : statistical order moment

Multifractal analysis using Wavelet Transform Modulus Maxima

Partition function: for a set $\mathcal{L}(a)$ of maxima lines

$$\mathcal{Z}(q, a) = \sum_{\ell \in \mathcal{L}(a)} \left(\sup_{(\mathbf{b}, a') \in \ell, a' \leq a} \mathbf{M}_\psi[f](\mathbf{b}, a') \right)^q$$

q : statistical order moment

Roughness, quantified by Hölder exponent, characterized by $\tau(q)$ spectrum

$$\mathcal{Z}(q, a) \sim a^{\tau(q)}, \quad a \rightarrow 0^+$$

For 2D fractional Brownian field: $\tau(q) = qH - 2$ is linear.

Multifractal analysis using Wavelet Transform Modulus Maxima

Partition function: for a set $\mathcal{L}(a)$ of maxima lines

$$\mathcal{Z}(q, a) = \sum_{\ell \in \mathcal{L}(a)} \left(\sup_{(\mathbf{b}, a') \in \ell, a' \leq a} \mathbf{M}_\psi[f](\mathbf{b}, a') \right)^q$$

q : statistical order moment

Roughness, quantified by Hölder exponent, characterized by $\tau(q)$ spectrum

$$\mathcal{Z}(q, a) \sim a^{\tau(q)}, \quad a \rightarrow 0^+$$

For 2D fractional Brownian field: $\tau(q) = qH - 2$ is linear.

Singularity spectrum: $\mathcal{D}(h)$ Haussdorff dimension of $\{x \in \mathbb{R}^2, h(x) = h\}$

$$\mathcal{D}(h) = \min_q (qh - \tau(q)) \quad (\text{Legendre transform of } \tau)$$

Multifractal analysis using Wavelet Transform Modulus Maxima

Numerically: unstable estimation of $\tau(q)$ and $\mathcal{D}(q)$

⇒ Mean quantities in a **canonical** ensemble with Boltzmann weights

$$W_\psi[f](q, \ell, a) = \frac{\left| \sup_{(\mathbf{b}, a') \in \ell, a' \leq a} \mathbf{M}_\psi[f](\mathbf{b}, a') \right|^q}{Z(q, a)}$$

Multifractal analysis using Wavelet Transform Modulus Maxima

Numerically: unstable estimation of $\tau(q)$ and $\mathcal{D}(q)$

⇒ Mean quantities in a **canonical** ensemble with Boltzmann weights

$$W_\psi[f](q, \ell, a) = \frac{\left| \sup_{(\mathbf{b}, a') \in \ell, a' \leq a} \mathbf{M}_\psi[f](\mathbf{b}, a') \right|^q}{Z(q, a)}$$

Roughness: robust local regularity estimation

$$h(q, a) = \sum_{\ell \in \mathcal{L}(a)} \ln \left(\left| \sup_{(\mathbf{b}, a') \in \ell, a' \leq a} \mathbf{M}_\psi[f](\mathbf{b}, a') \right| \right) W_\psi[f](q, \ell, a),$$

$$h(q) = \frac{d\tau}{dq} = \lim_{a \rightarrow 0^+} \frac{h(q, a)}{\ln a}$$

Multifractal analysis using Wavelet Transform Modulus Maxima

Numerically: unstable estimation of $\tau(q)$ and $\mathcal{D}(q)$

⇒ Mean quantities in a **canonical** ensemble with Boltzmann weights

$$W_\psi[f](q, \ell, a) = \frac{\left| \sup_{(\mathbf{b}, a') \in \ell, a' \leq a} \mathbf{M}_\psi[f](\mathbf{b}, a') \right|^q}{Z(q, a)}$$

Roughness: robust local regularity estimation

$$\begin{aligned} h(q, a) &= \sum_{\ell \in \mathfrak{L}(a)} \ln \left(\left| \sup_{(\mathbf{b}, a') \in \ell, a' \leq a} \mathbf{M}_\psi[f](\mathbf{b}, a') \right| \right) W_\psi[f](q, \ell, a), \\ h(q) &= \frac{d\tau}{dq} = \lim_{a \rightarrow 0^+} \frac{h(q, a)}{\ln a} \end{aligned}$$

Singularity spectrum:

$$\begin{aligned} \mathcal{D}(q, a) &= \sum_{\ell \in \mathfrak{L}(a)} \ln (W_\psi[f](q, \ell, a)) W_\psi[f](q, \ell, a), \\ \mathcal{D}(q) &= \lim_{a \rightarrow 0^+} \frac{\mathcal{D}(q, a)}{\ln a} \end{aligned}$$

Patch-wise fractal analysis of mammographic breast tissue

$$\text{Roughness: } h(q) = \lim_{a \rightarrow 0^+} \frac{h(q, a)}{\ln a}; \quad \text{Singularity spectrum: } \mathcal{D}(q, a) = \lim_{a \rightarrow 0^+} \frac{\mathcal{D}(q, a)}{\ln a}$$

- The larger the patch, the larger the range of q values, the better the estimate;
 - but risk of confusing average of several monofractal signatures and multifractal.
- ⇒ estimation on overlapping patches of size 360×360 pixels with 32-pixel shift

$$\text{Roughness: } h(q) = \lim_{a \rightarrow 0^+} \frac{h(q, a)}{\ln a};$$

$$\text{Singularity spectrum: } \mathcal{D}(q, a) = \lim_{a \rightarrow 0^+} \frac{\mathcal{D}(q, a)}{\ln a}$$

- The larger the patch, the larger the range of q values, the better the estimate;
- but risk of confusing average of several monofractal signatures and multifractal.
⇒ estimation on overlapping patches of size 360×360 pixels with 32-pixel shift

Image sliding window analysis

1. Check that the central 256×256 pixels are contained in the mask;
2. if so, compute the Wavelet Transform for 50 scales, from $a = 7$ to 120 pixels;
3. extract the space-scale skeleton from the central 256×256 pixels;
4. compute $h(q, a)$ and $\mathcal{D}(q, a)$ from the partition function $\mathcal{Z}(q, a)$;
5. linear regressions $h(q, a)$ vs. $\log_2(a)$ and $\mathcal{D}(q, a)$ vs. $\log_2(a)$:
how to choose the range of scales $[a_{\min}, a_{\max}]$?

Patch-wise fractal analysis of mammographic breast tissue

For **each** patch of 360×360 pixels, i.e., 15.5×15.5 mm

$$\text{roughness: } h(q) = \lim_{a \rightarrow 0^+} \frac{h(q, a)}{\ln a}; \quad \text{singularity spectrum: } \mathcal{D}(q, a) = \lim_{a \rightarrow 0^+} \frac{\mathcal{D}(q, a)}{\ln a}$$

\implies linear regressions $h(q, a)$ vs. $\log_2(a)$ and $\mathcal{D}(q, a)$ vs. $\log_2(a)$ across $[a_{\min}, a_{\max}]$

Patch-wise fractal analysis of mammographic breast tissue

For **each** patch of 360×360 pixels, i.e., 15.5×15.5 mm

$$\text{roughness: } h(q) = \lim_{a \rightarrow 0^+} \frac{h(q, a)}{\ln a}; \quad \text{singularity spectrum: } \mathcal{D}(q, a) = \lim_{a \rightarrow 0^+} \frac{\mathcal{D}(q, a)}{\ln a}$$

\Rightarrow linear regressions $h(q, a)$ vs. $\log_2(a)$ and $\mathcal{D}(q, a)$ vs. $\log_2(a)$ across $[a_{\min}, a_{\max}]$

The Autofit Methodology: imposing $\log_2 a_{\max} - \log_2 a_{\min} \geq 1$ explore

$$\log_2 \frac{a_{\min}}{\sigma_w} = 0.0, 0.1, \dots, 2.1, , \quad \log_2 \frac{a_{\max}}{\sigma_w} = 2.0, 2.1, \dots, 4.1, \quad \text{with } \sigma_w = 7 \text{ pixels}$$

and select $[a_{\min}, a_{\max}]$ if and only if

Patch-wise fractal analysis of mammographic breast tissue

For **each** patch of 360×360 pixels, i.e., 15.5×15.5 mm

$$\text{roughness: } h(q) = \lim_{a \rightarrow 0^+} \frac{h(q, a)}{\ln a}; \quad \text{singularity spectrum: } \mathcal{D}(q, a) = \lim_{a \rightarrow 0^+} \frac{\mathcal{D}(q, a)}{\ln a}$$

\Rightarrow linear regressions $h(q, a)$ vs. $\log_2(a)$ and $\mathcal{D}(q, a)$ vs. $\log_2(a)$ across $[a_{\min}, a_{\max}]$

The Autofit Methodology: imposing $\log_2 a_{\max} - \log_2 a_{\min} \geq 1$ explore

$$\log_2 \frac{a_{\min}}{\sigma_w} = 0.0, 0.1, \dots, 2.1, , \quad \log_2 \frac{a_{\max}}{\sigma_w} = 2.0, 2.1, \dots, 4.1, \quad \text{with } \sigma_w = 7 \text{ pixels}$$

and select $[a_{\min}, a_{\max}]$ if and only if

- linear regression on $h(q = 0, a)$ from a_{\min} to a_{\max} yields

$$-0.2 < \hat{h}(q = 0) = \hat{H} < 1$$

- $H \leq -0.2$: high roughness \Rightarrow abnormally high noise
- $H \geq 1$: low roughness, differentiable field \Rightarrow artificially smooth

Patch-wise fractal analysis of mammographic breast tissue

For **each** patch of 360×360 pixels, i.e., 15.5×15.5 mm

$$\text{roughness: } h(q) = \lim_{a \rightarrow 0^+} \frac{h(q, a)}{\ln a}; \quad \text{singularity spectrum: } \mathcal{D}(q, a) = \lim_{a \rightarrow 0^+} \frac{\mathcal{D}(q, a)}{\ln a}$$

\Rightarrow linear regressions $h(q, a)$ vs. $\log_2(a)$ and $\mathcal{D}(q, a)$ vs. $\log_2(a)$ across $[a_{\min}, a_{\max}]$

The Autofit Methodology: imposing $\log_2 a_{\max} - \log_2 a_{\min} \geq 1$ explore

$$\log_2 \frac{a_{\min}}{\sigma_w} = 0.0, 0.1, \dots, 2.1, , \quad \log_2 \frac{a_{\max}}{\sigma_w} = 2.0, 2.1, \dots, 4.1, \quad \text{with } \sigma_w = 7 \text{ pixels}$$

and select $[a_{\min}, a_{\max}]$ if and only if

- linear regression on $\mathcal{D}(q = 0, a)$ from a_{\min} to a_{\max} yields

$$1.7 < \hat{\mathcal{D}}(h(q = 0)) < 2.5$$

for a monofractal field of Hurst exponent H , expected to be $\mathcal{D}(H) = 2$

but finite size effect affect the maxima lines as $a \rightarrow 0^+$

Patch-wise fractal analysis of mammographic breast tissue

For **each** patch of 360×360 pixels, i.e., 15.5×15.5 mm

$$\text{roughness: } h(q) = \lim_{a \rightarrow 0^+} \frac{h(q, a)}{\ln a}; \quad \text{singularity spectrum: } \mathcal{D}(q, a) = \lim_{a \rightarrow 0^+} \frac{\mathcal{D}(q, a)}{\ln a}$$

\Rightarrow linear regressions $h(q, a)$ vs. $\log_2(a)$ and $\mathcal{D}(q, a)$ vs. $\log_2(a)$ across $[a_{\min}, a_{\max}]$

The Autofit Methodology: imposing $\log_2 a_{\max} - \log_2 a_{\min} \geq 1$ explore

$$\log_2 \frac{a_{\min}}{\sigma_w} = 0.0, 0.1, \dots, 2.1, , \quad \log_2 \frac{a_{\max}}{\sigma_w} = 2.0, 2.1, \dots, 4.1, \quad \text{with } \sigma_w = 7 \text{ pixels}$$

and select $[a_{\min}, a_{\max}]$ if and only if

- coefficient of determination of linear regression on $h(q = 0, a)$ from a_{\min} to a_{\max}

$$R^2 > 0.96$$

sufficiently linear to extract the Hurst exponent H

Patch-wise fractal analysis of mammographic breast tissue

For **each** patch of 360×360 pixels, i.e., 15.5×15.5 mm

$$\text{roughness: } h(q) = \lim_{a \rightarrow 0^+} \frac{h(q, a)}{\ln a}; \quad \text{singularity spectrum: } \mathcal{D}(q, a) = \lim_{a \rightarrow 0^+} \frac{\mathcal{D}(q, a)}{\ln a}$$

\Rightarrow linear regressions $h(q, a)$ vs. $\log_2(a)$ and $\mathcal{D}(q, a)$ vs. $\log_2(a)$ across $[a_{\min}, a_{\max}]$

The Autofit Methodology: imposing $\log_2 a_{\max} - \log_2 a_{\min} \geq 1$ explore

$$\log_2 \frac{a_{\min}}{\sigma_w} = 0.0, 0.1, \dots, 2.1, , \quad \log_2 \frac{a_{\max}}{\sigma_w} = 2.0, 2.1, \dots, 4.1, \quad \text{with } \sigma_w = 7 \text{ pixels}$$

and select $[a_{\min}, a_{\max}]$ if and only if

- weighted standard deviation across q of the $\widehat{h}(q)$ estimated from a_{\min} to a_{\max}

$$sd_w < 0.06$$

\Rightarrow excludes multifractal scaling

q	-2	-1.5	-1	-0.5	-0.3	-0.2	-0.1	0	0.1	0.2	0.3	0.5	1	1.5	2	2.5	3
w	0.1	0.5	1	3	5	7	9	10	9	8	7	5	3	2	1	0.5	0.2

Patch-wise fractal analysis of mammographic breast tissue

For **each** patch of 360×360 pixels, i.e., 15.5×15.5 mm

$$\text{roughness: } h(q) = \lim_{a \rightarrow 0^+} \frac{h(q, a)}{\ln a}; \quad \text{singularity spectrum: } \mathcal{D}(q, a) = \lim_{a \rightarrow 0^+} \frac{\mathcal{D}(q, a)}{\ln a}$$

\Rightarrow linear regressions $h(q, a)$ vs. $\log_2(a)$ and $\mathcal{D}(q, a)$ vs. $\log_2(a)$ across $[a_{\min}, a_{\max}]$

The Autofit Methodology: imposing $\log_2 a_{\max} - \log_2 a_{\min} \geq 1$ explore

$$\log_2 \frac{a_{\min}}{\sigma_w} = 0.0, 0.1, \dots, 2.1, , \quad \log_2 \frac{a_{\max}}{\sigma_w} = 2.0, 2.1, \dots, 4.1, \quad \text{with } \sigma_w = 7 \text{ pixels}$$

and select $[a_{\min}, a_{\max}]$ if and only if

- weighted average of goodness of fit of $\hat{h}(q)$ estimated from a_{\min} to a_{\max}

$$\langle R_w^2 \rangle > 0.96$$

\Rightarrow ensures self-similarity

q	-2	-1.5	-1	-0.5	-0.3	-0.2	-0.1	0	0.1	0.2	0.3	0.5	1	1.5	2	2.5	3
w	0.1	0.5	1	3	5	7	9	10	9	8	7	5	3	2	1	0.5	0.2

Patch-wise fractal analysis of mammographic breast tissue

For **each** patch of 360×360 pixels:

⇒ linear regressions $h(q, a)$ vs. $\log_2(a)$ and $D(q, a)$ vs. $\log_2(a)$ across $[a_{\min}, a_{\max}]$

The Autofit Methodology: imposing $\log_2 a_{\max} - \log_2 a_{\min} \geq 1$ explore **418 couples**

$$\log_2 \frac{a_{\min}}{\sigma_w} = 0.0, 0.1, \dots, 2.1, , \quad \log_2 \frac{a_{\max}}{\sigma_w} = 2.0, 2.1, \dots, 4.1, \text{ with } \sigma_w = 7 \text{ pixels}$$

and select $[a_{\min}, a_{\max}]$ if and only if

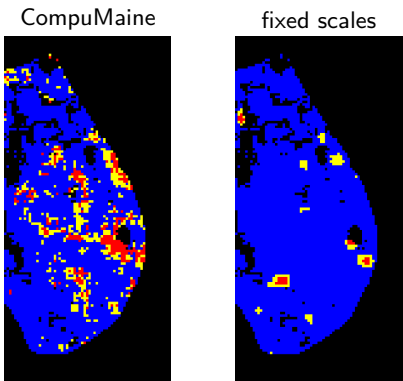
- $-0.2 < h(q = 0) < 1$: expected roughness
- $1.7 < \hat{D} < 2.5$: expect 2
- $R^2 > 0.96$: accurate estimation of H
- $sd_w < 0.06$: monofractal scaling
- $\langle R_w^2 \rangle > 0.96$: $h(q, a)$ sufficiently linear

⇒ If no scale range $[a_{\min}, a_{\max}]$ for which all conditions are satisfied: **no scaling**.

Patch-wise fractal analysis of mammographic breast tissue

Wavelet leader coefficients (Wendt et al., 2009, Sig. Process.)

- $H < 1/2$ monofractal anti-correlated: fatty tissues (healthy)
- $H > 1/2$ monofractal long-range correlated: dense tissues (healthy)
- $H \simeq 1/2$ monofractal uncorrelated: disrupted tissues (tumorous)

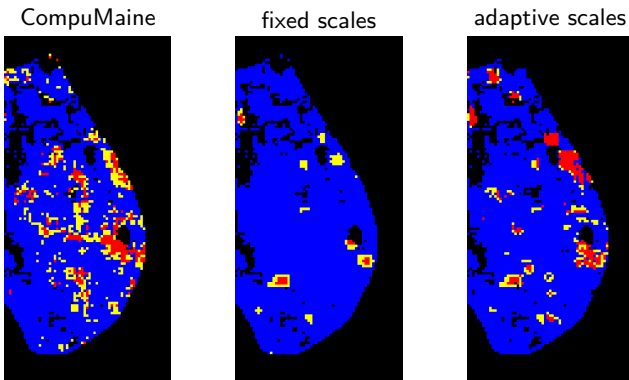


$$[a_{\min}, a_{\max}] = [2^3, 2^5]$$

Patch-wise fractal analysis of mammographic breast tissue

Wavelet leader coefficients (Wendt et al., 2009, Sig. Process.)

- $H < 1/2$ monofractal anti-correlated: fatty tissues (healthy)
- $H > 1/2$ monofractal long-range correlated: dense tissues (healthy)
- $H \simeq 1/2$ monofractal uncorrelated: disrupted tissues (tumorous)

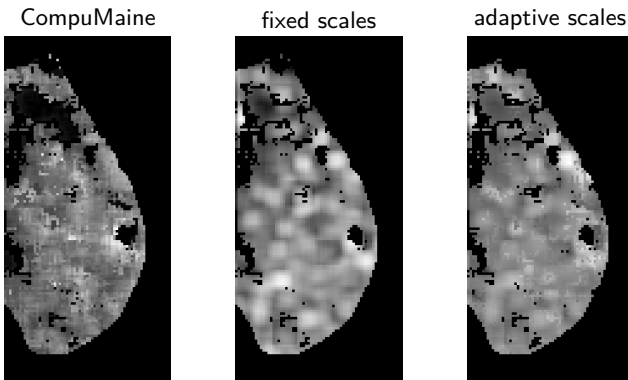


$$[a_{\min}, a_{\max}] = [2^3, 2^5] \quad [a_{\min}, a_{\max}] \subset [2^2, 2^8]$$

Patch-wise fractal analysis of mammographic breast tissue

Wavelet leader coefficients (Wendt et al., 2009, Sig. Process.)

- $H < 1/2$ monofractal anti-correlated: fatty tissues (healthy)
- $H > 1/2$ monofractal long-range correlated: dense tissues (healthy)
- $H \simeq 1/2$ monofractal uncorrelated: disrupted tissues (tumorous)



$$[a_{\min}, a_{\max}] = [2^3, 2^5] \quad [a_{\min}, a_{\max}] \subset [2^2, 2^8]$$

Mammogram datasets

Marin et al., 2017, *Phys. Med. Biol.*

DDSM: University of South Florida, Digital Database for Screening Mammography

43 normal vs. 49 cancer, 35 benign

⇒ digitized films: lossless JPEG 12-bit images (pixel values: integers in [0, 4095])

Tumorous breasts have more disrupted tissues compared to normal breasts:

normal vs. cancer: $P \sim 0.0023$, normal vs. benign: $P \sim 0.0049$.

Mammogram datasets

Marin et al., 2017, *Phys. Med. Biol.*

DDSM: University of South Florida, Digital Database for Screening Mammography

43 normal vs. 49 cancer, 35 benign

⇒ digitized films: lossless JPEG 12-bit images (pixel values: integers in [0, 4095])

Tumorous breasts have more disrupted tissues compared to normal breasts:

normal vs. cancer: $P \sim 0.0023$, normal vs. benign: $P \sim 0.0049$.

Gerasimova-Chechkina et al., 2021, *Front. Physiol.*

Russian: Perm Regional Oncological Dispensary

81 cancer vs. 23 benign

⇒ digitally acquired mammograms: uncompressed 8-bit BMP images ([0, 255])

Cancerous breasts have more disrupted tissues compared to breasts with benign lesions:

cancer vs. benign: $P \sim 0.003$

Mammogram datasets

Marin et al., 2017, *Phys. Med. Biol.*

DDSM: University of South Florida, Digital Database for Screening Mammography

43 normal vs. 49 cancer, 35 benign

⇒ digitized films: lossless JPEG 12-bit images (pixel values: integers in [0, 4095])

Tumorous breasts have more disrupted tissues compared to normal breasts:

normal vs. cancer: $P \sim 0.0023$, normal vs. benign: $P \sim 0.0049$.

Gerasimova-Chechkina et al., 2021, *Front. Physiol.* ⇒ shared with us, with analyses

Russian: Perm Regional Oncological Dispensary

81 cancer vs. 23 benign

⇒ digitally acquired mammograms: uncompressed 8-bit BMP images ([0, 255])

Cancerous breasts have more disrupted tissues compared to breasts with benign lesions:

cancer vs. benign: $P \sim 0.003$

Mammogram datasets

Gerasimova-Chechkina et al., 2021, *Front. Physiol.* \Rightarrow shared with us, with analyses

Russian: *Perm Regional Oncological Dispensary*

81 cancer vs. 23 benign

\Rightarrow digitally acquired mammograms: uncompressed 8-bit BMP images ([0, 255])

Cancerous breasts have more disrupted tissues compared to breasts with benign lesions:

cancer vs. benign: $P \sim 0.003$

Mammogram datasets

Gerasimova-Chechkina et al., 2021, *Front. Physiol.* \Rightarrow shared with us, with analyses

Russian: *Perm Regional Oncological Dispensary*

81 cancer vs. 23 benign

\Rightarrow digitally acquired mammograms: uncompressed 8-bit BMP images ([0, 255])

Cancerous breasts have more disrupted tissues compared to breasts with benign lesions:

cancer vs. benign: $P \sim 0.003$

Patch-wise analysis with wavelet leaders

- Daubechies wavelets with $n_\psi = 2$ vanishing moments
- \sim scales selected by the CompuMaine autofit method, up to rounding errors

Mammogram datasets

Gerasimova-Chechkina et al., 2021, *Front. Physiol.* \Rightarrow shared with us, with analyses

Russian: *Perm Regional Oncological Dispensary*

81 cancer vs. 23 benign

\Rightarrow digitally acquired mammograms: uncompressed 8-bit BMP images ([0, 255])

Cancerous breasts have more disrupted tissues compared to breasts with benign lesions:

cancer vs. benign: $P \sim 0.003$

Patch-wise analysis with wavelet leaders

- Daubechies wavelets with $n_\psi = 2$ vanishing moments
- \sim scales selected by the CompuMaine autofit method, up to rounding errors

cancer vs. benign: $P \sim 0.074$

Conclusions

Patch-wise fractal analysis of mammograms with WT modulus maxima method

- disrupted tissues, characterized by $H \sim 1/2$, indicate loss of homeostasis
- quantity of disrupted tissues discriminates between

(Marin et al., 2017) tumorous vs. normal $P \sim 0.0006$

(Gerasimova-Chechkina et al., 2021) cancer vs. benign $P \sim 0.0030$

⇒ exploration of 418 couples of (a_{\min}, a_{\max}) for each patch and strict conditions

Conclusions

Patch-wise fractal analysis of mammograms with WT modulus maxima method

- disrupted tissues, characterized by $H \sim 1/2$, indicate loss of homeostasis
- quantity of disrupted tissues discriminates between

(Marin et al., 2017) tumorous vs. normal $P \sim 0.0006$

(Gerasimova-Chechkina et al., 2021) cancer vs. benign $P \sim 0.0030$

⇒ exploration of 418 couples of (a_{\min}, a_{\max}) for each patch and strict conditions

Reproduction with wavelet leaders formalism on Russian dataset

- range of scales for each patch extracted from CompuMaine analyses,
- remains less informative: $P \sim 0.0740$

From patch-wise to pixel-wise fractal analysis

- using wavelet leaders framework,
- combined with variational methods,
- with PyTorch implementation to benefit from fast GPU computing,
- reduced number of hyperparameters & fine-tuned automatically

⇒ increase the sensibility in the measurement of the quantity of disrupted tissues

From patch-wise to pixel-wise fractal analysis

- using wavelet leaders framework,
 - combined with variational methods,
 - with PyTorch implementation to benefit from fast GPU computing,
 - reduced number of hyperparameters & fine-tuned automatically
- ⇒ increase the sensibility in the measurement of the quantity of disrupted tissues

Anisotropic Gaussian fields for mammogram modeling

- observed in Richard & Biermé, 2010, *J. Math. Imaging Vis.*,
- many tools that have never been applied to mammograms yet:

Biermé, Carré, Lacaux, & Launay, 2024, hal-04659825

- other mammograms datasets: VinDr-Mammo.